MEASURING TRACE GASES IN PLUMES FROM HYPERSPECTRAL REMOTELY SENSED DATA

Rodolphe Marion,[1, 2] Rémi Michel,[1] and Christian Faye[2]

1. INTRODUCTION

Characterizing surface and atmospheric properties from hyperspectral imaging spectrometry is of major importance in earth sciences. It has been successfully applied to geological, aquatic, ecological and atmospheric research (Curran, 1994) (Goetz, 1992).

Hyperspectral sensors (e.g., AVIRIS, HyMap, Hyperion) are passive earth-looking systems providing radiance images in the solar reflected portion of the electromagnetic radiation spectrum. Generally, they cover a spectral range included in the 400–2500 nm window with a few hundred contiguous bands about 10 nm wide. The nominal pixel size is about 20 m. Typical signal to noise ratios (SNR) are a few hundred. As an example, the AVIRIS spectral range is 400–2500 nm, the number of bands is 224, the spectral bands are about 10 nm wide, the spatial resolution is about 20 m, and the SNR is between 300 and 800 for the year 1995. The images depend on sun irradiance, atmospheric conditions, ground conditions, and on the system's transfer function in a complex way (scattering, absorption, reflection, averaging), leading to a strongly non-linear pixel equation (3). Fig. 1 shows a diagram of the hyperspectral observational geometry.

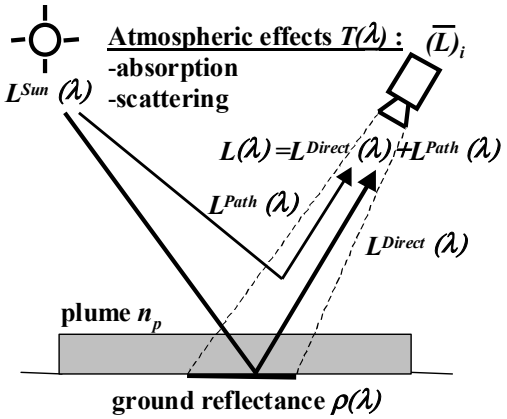

Figure 1. Hyperspectral data collection. Sun emitted electromagnetic wave $L^{Sun}(\lambda)$ interacts with atmospheric molecules and particles through absorption and scattering processes ($T(\lambda)$). At-sensor radiance $L(\lambda)$ is the sum of ground reflected radiance $L^{Direct}(\lambda)$ and backscattered atmospheric radiance $L^{Path}(\lambda)$. Radiance is band-averaged by the instrument, yielding measured signal $(\bar{L})_i$ for spectral channel i. This signal includes spectral features of effluent plume n_p.

One of the major issues of hyperspectral data processing is the joint retrieval of atmospheric gas concentrations and ground reflectance. It is essential not only for studying atmospheric properties but also for ground based applications requiring accurate atmospheric correction (Curran, 1994) (Goetz, 1992). Several techniques have already been proposed to measure the amount of a particular gas of interest (e.g., H_2O, CO_2, O_2, O_3) including : narrow/wide ratio, N/W (Frouin et al., 1990a) (Frouin et al., 1990b), continuum interpolated band ratio, CIBR (Green et al., 1989) (Bruegge et al., 1990) (Kaufman et al., 1992), atmospheric precorrected differential absorption technique, APDA (Borel et al., 1996) (Schläpfer et al., 1996a) (Schläpfer et al., 1998), linear regression ratio, LIRR (a variation of the CIBR introduced by Schläpfer et al., 1996b), and curve-fitting procedures (Gao et al., 1990). These methods typically yield the total water vapor content with an accuracy of about 7% rms from AVIRIS data. Accuracy may decline to more than several tens of a percent when the ground reflectance varies non-linearly with wavelength within gas absorption bands (Borel et al., 1996) (Schläpfer et al., 1998), or when other species than water are considered (Schläpfer et al., 1996b) (Green et al., 1996b) (De Jong et al., 1996). A more accurate estimation of gas amounts is generally required to investigate a wider range of phenomena including forest fires, volcanoes, and industrial pollution.

Hereafter, we first present those principles of imaging spectrometry useful for yielding the equation of the image. We then discuss the potential and the limitations of the existing methods, especially when the unknown surface reflectance varies non-linearly with wavelength within gas absorption bands. Afterwards, we propose an

[1] CEA-DIF-DASE-LDG-TSE, BP 12, 91680 Bruyères-le-Châtel Cedex, France (rodolphe.marion@cea.fr)
[2] ENSEA-ETIS, 6 avenue du Ponceau, 95014 Cergy-Pontoise Cedex, France

enhanced method, named Joint Reflectance and Gas Estimator, JRGE. It is dedicated to the measurement of trace gases within a plume corresponding to variations relative to a given standard atmosphere model. This method is based on a cubic smoothing spline-like surface reflectance estimator and non-linear radiative transfer calculations. Finally, JRGE is applied to simulated data as preliminary results. An aerosol-free atmosphere (Rayleigh atmosphere) and standard ground temperatures are assumed.

2. IMAGING SPECTROMETRY

From the viewing geometry schematically shown in Fig. 1, the monochromatic radiance at the input of a downward looking sensor can be written in a simplified form as (Esaias, 1986)

$$L(\lambda) = \rho(\lambda) L^{Sun}(\lambda) T(\lambda) + L^{Path}(\lambda) \tag{1}$$

where λ is the wavelength, $L(\lambda)$ is the radiance at the imaging spectrometer, $\rho(\lambda)$ is the surface reflectance, $L^{Sun}(\lambda)$ is the solar radiance above the atmosphere; $T(\lambda)$ is the total atmospheric transmittance, equal to the product of the atmospheric transmittance from the sun to the earth's surface and from the earth's surface to the sensor, according to the Beer-Bouguer-Lambert law (Liou, 1980); and $L^{Path}(\lambda)$ is the path-scattered radiance (i.e., the backscattered atmospheric radiance not reflected by the ground).

In the presence of a plume located just above the ground (typically in the first kilometer of the atmosphere) containing P gaseous species in addition to the standard atmospheric state, the at-sensor radiance becomes

$$L(\lambda, n_1, ..., n_P) = \rho(\lambda) L^{Sun}(\lambda) T(\lambda) \exp\left(-\eta \sum_{p=1}^{P} k_p(\lambda) n_p \right) + L^{Path}(\lambda, n_1, ..., n_P) \tag{2}$$

where $n_p, p = 1,...,P$, is the integrated density over the plume height of the pth species, η is a known geometrical parameter depending on the viewing angles (i.e., sun and sensor locations), $k_p(\lambda)$ is the known absorption coefficient (altitude-dependant) of the pth species, and $\exp\left(-\eta \sum_{p=1}^{P} k_p(\lambda) n_p\right)$ is the total plume transmittance. The path-scattered radiance L^{Path} is also a function of the unknown gas densities. The total atmospheric content in the pth species can be written $N_p = N_{0p} + n_p$ where N_{0p} represents the standard atmospheric density and n_p is the unknown excess due to the plume.

A hyperspectral sensor performs a band-averaging $(\overline{L})_i$ of the incoming radiance field $L(\lambda)$ at each channel i ($i = 1,...,N$, N is the total number of channels of the imaging system). This measure, corrupted by the additive noise b_i is then equal to

$$\begin{aligned} \left(\overline{L(n_1,...,n_P)}\right)_i &= \int_0^\infty L(\lambda, n_1, ..., n_P) H_i(\lambda) d\lambda + b_i \\ &= \left(\overline{\rho L^{Sun} T \exp\left(-\eta \sum_{p=1}^{P} k_p n_p \right)} \right)_i + \left(\overline{L^{Path}(n_1,...,n_P)}\right)_i + b_i \end{aligned} \tag{3}$$

where H_i is the normalized instrument's transfer function for channel i. The spectral atmospheric features are typically tenths narrower than the instrument channel width (e.g., H_2O absorption bands near 1 μm are about 10^{-3} nm wide and AVIRIS spectral channel width is about 10 nm). It is thus noteworthy that the multiplicative operator of monochromatic atmospheric terms in equation (3) does not commute with the instrument averaging operator.

According to the properties of surface reflectance spectra (see section 4.1) and by defining $A_0(\lambda) = L^{Sun}(\lambda) T(\lambda)$, the measured radiance of a pixel for channel i can be written

$$\left(\overline{L(n_1,...,n_P)}\right)_i = \rho_i \left(\overline{A_0 \exp\left(-\eta \sum_{p=1}^{P} k_p n_p \right)} \right)_i + \left(\overline{L^{Path}(n_1,...,n_P)}\right)_i + b_i \tag{4}$$

where ρ_i is the mean ground reflectance over the channel i. Theoretically, L^{Path} depends on n_p, drastically increasing the complexity of the model. In our approach, we determine an excess of gases due to the plume and not the total atmospheric content so that L^{Path} can be considered independent of n_p. The measured radiance of a pixel for channel i can thus be written as

$$\left(\overline{L(n_1,...,n_P)}\right)_i = \rho_i \left(\overline{A_0 \exp\left(-\eta \sum_{p=1}^{P} k_p n_p \right)} \right)_i + \left(\overline{L^{Path}}\right)_i + b_i \,. \quad (5)$$

Hereafter, we propose a method to estimate the $n_p, p = 1,...,P$, from equation (5) for which the $\rho_i, i = 1,...,N$, are unknown, η and $k_p, p = 1,...,P$, are known, A_0 and L^{Path} are computed from a standard atmosphere model, and a noise model is available (see section 4.1).

3. POTENTIAL AND LIMITS OF CONVENTIONAL METHODS

Existing methods have extensively been applied to hyperspectral data, especially AVIRIS images, to retrieve the water vapor column (Green et al., 1989) and, with less accuracy, the ozone (Schläpfer et al., 1996b), oxygen (Green et al., 1996b), and carbon dioxide (De Jong et al., 1996) columns. For a comparison between these methods see e.g., (Carrère et al., 1993 for N/W and CIBR) and (Schläpfer et al., 1998 for CIBR and APDA). Ratioing and curve-fitting techniques are shown to suffer from limitations including (i) the assumed linear variations of the surface reflectance within gas absorption bands, (ii) the assumption of non-overlapping gas absorption bands, and (iii) the need for a high SNR at each side of the gas absorption bands. These limitations may yield a typical error far greater than 10% in H_2O column density retrieval over some ground materials (see (Borel et al., 1996) and (Schläpfer et al., 1998) for a validation of APDA over 379 reflectance spectra).

3.1 Effect of Non-linearity of the Reflectance ρ within Gas Absorption Bands

The reflectance spectrum of enstatite (sample IN-10B, particle size 45-125 µm) was chosen as a reference (from the Jet Propulsion Laboratory (JPL), Pasadena, CA, spectral library) because it is frequently encountered on the earth's surface and because of the high error of standard methods for this material. A radiance pixel was simulated using MODTRAN4 in the single scattering mode with the following entries: aerosol-free US 1976 Standard Atmosphere Model with an excess of water vapor equal to 3500 ppm in the first atmospheric kilometer (to simulate a vapor plume), solar zenith angle of 40 degrees, target at sea level, and nadir viewing sensor located above the atmosphere. Noise was added to the computed signal using the radiometric characteristics of the AVIRIS instrument for the year 1995 (see section 4.1). We used the 3-channel optimal APDA technique (reference channels: 875.25 nm / FWHM = 8.86 nm and 1000.13 nm / FWHM = 9.01 nm, measurement channel : 942.49 nm / FWHM = 8.95 nm) applied to the 940 nm water vapor absorption band (Fig. 2) (FWHM is the Full Width at Half-Maximum).

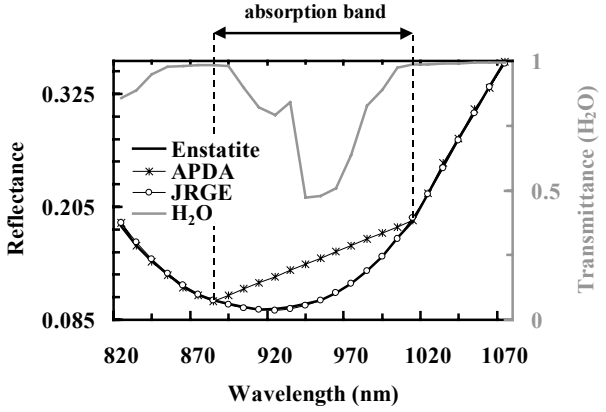

Figure 2. H_2O retrieval around 940 nm absorption band (grey line) over enstatite (black line). APDA linear interpolation (black stars) yields overestimation of reflectance and 41% overdetermined H_2O content. JRGE proposed method better fits parabolic enstatite shape (white circles) and reduces error on H_2O to 6% (see text for details).

Like other conventional methods, APDA first performs a linear interpolation of ρ within absorption bands. This assumption yields an overestimation of ρ reaching about 43% in the center of the 940 nm absorption band, leading to an estimated H_2O excess equal to 12,880 ppm instead of 3500 ppm. It corresponds to a relative error

in the first atmospheric layer equal to 268%. This error in the total atmospheric H_2O content is about 41%. This overdetermined value is due to the parabolic shape of enstatite near 940 nm. This example illustrates that the usual assumption of linear variations of ρ within absorption bands may yield large errors.

3.2 Effect of Overlapping Absorption Bands

Conventional methods use the assumption of separated gas absorption bands and estimate each n_p separately. However, absorption bands may overlap (Fig. 3) so that one may be in need for a more comprehensive method of retrieving simultaneously the n_p.

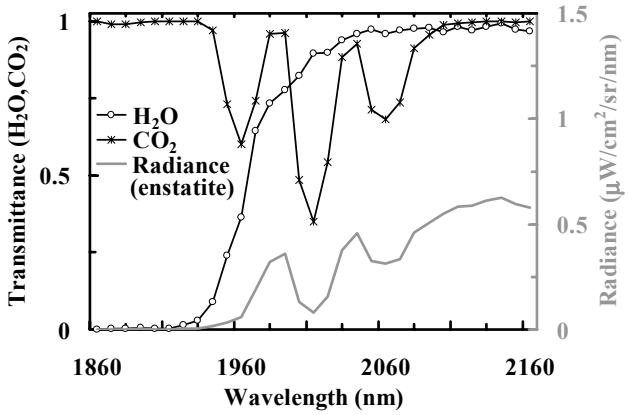

Figure 3. H_2O and CO_2 overlapping absorption bands near 2000 nm (white circles and black stars, respectively) yield a complex radiance pattern (grey line). Contrary to previous standard algorithms, JRGE addresses that point in a simultaneous gases retrieval procedure.

3.3 Effect of Noise

Conventional methods use a few reference channels located at each side of the absorption bands in order to interpolate the surface reflectance. The interpolation thus drastically depends on the noise in these reference channels. They do not benefit from the whole signal to minimize the influence of noise during the reflectance interpolation procedure. This point is generally negligible for H_2O retrieval but may be of high importance for CO_2 retrieval, with absorption bands located in low SNR spectral regions.

4. JRGE : THEORETICAL DEVELOPMENTS

In the following, we propose a method that overcomes the main drawbacks of the conventional methods listed above. It is based on a mathematical description of the physical characteristics of the signal. The developed algorithm is a two-step algorithm that first estimates the surface reflectance and then the densities of the plume gases.

4.1 Physical Constraints and Assumptions

We consider the following physical constraints and assumptions :

- From imaging spectrometry theory (Goetz, 1992), surface reflectance spectra generally do not include hyperfine absorption features. For current hyperspectral sensors (e.g., AVIRIS, HyMap, Hyperion), the surface reflectance can thus be considered as a spectrally smooth function of wavelength. This assumption allows (i) consideration of reflectance values at channel center in equation (4) and (ii) the construction of the proposed estimator.
- Estimates of the minimum and maximum values of n_p ($n_{p\min}$ and $n_{p\max}$, respectively) are available. As an example, the user may suggest that N_{0p} represents N_p with an accuracy of 20, 30, or 100%, or may give values depending on the studied phenomenon (e.g., forest fire, volcano, industrial plant). This requirement will allow the selection of the measurement (or absorption) channels (see section 4.2).
- A noise model is assumed to be available. The total noise on the measured radiance in channel i results from two independent noise contributions: (i) the inherent photon noise and (ii) the instrument's noise. The

total noise can be modeled by an additive gaussian white noise process b_i with zero mean and a standard deviation equal to σ_{bi}; the noises in the different channels are supposed to be statistically independent (Green et al., 1996a). The photon noise is estimated from the conversion factor of photons to signal, and the instrument's noise is defined as the standard deviation of the dark signal measured during the image acquisition ((Green et al., 1996a) and (Vane et al., 1987) for AVIRIS sensor specifications), so that an estimate of the noise standard deviation is available for each channel of each pixel. Typical SNR values are greater than 500 over much of the spectral range for 1995 AVIRIS data (between 300 and 800).

- The gases of interest are known and characterized by their absorption coefficient k_p, calculated from spectroscopic data obtained in (Rothman et al., 1998).
- The terms A_0 and L^{Path} are computed in standard atmospheric conditions using a line-by-line radiative transfer code before applying sensor averaging.

4.2 Channel Selection

The proposed method considers three types of channels (Fig. 4):

4.2.1 Measurement Channels

Measurement (or absorption) channels are the channels of the imaging system sensitive to variations in the amount of trace gases. First, an equivalent reflectance $\tilde{\rho}_i$ is computed from the data $\left(\overline{L(n_1,...,n_P)}\right)_i$ and equation (5) under the assumption of zero n_p (Fig. 4) :

$$\tilde{\rho}_i = \frac{\left(\overline{L(n_1,...,n_P)}\right)_i - \left(\overline{L^{Path}}\right)_i}{\left(\overline{A_0}\right)_i}. \tag{6}$$

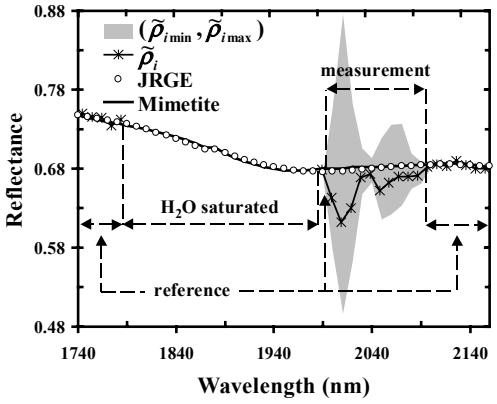

Figure 4. Spectral channels definition and selection. Standard atmospheric parameters and physical assumptions (see text for details) yield equivalent, minimum, and maximum estimates of reflectance from radiance signal (black stars and grey shape, respectively). $(\tilde{\rho}_{i\max} - \tilde{\rho}_{i\min})$ variations below noise define reference channels. Radiance below noise yields saturated channels. Gas-dependant channels are referred to as measurement channels. JRGE interpolation (white circles) constraints depend on channel type.

The associated standard deviation σ_i is related to the radiance standard deviation σ_{bi} by $\sigma_i = \sigma_{bi} \Big/ \left(\overline{A_0}\right)_i$. Similarly, the minimum and the maximum values of the reflectance ($\tilde{\rho}_{i\min}$ and $\tilde{\rho}_{i\max}$, respectively) are computed from the assumed variations $n_{p\min}$ and $n_{p\max}$ of n_p and equation (5)

$$\tilde{\rho}_{i\min} = \frac{\left(\overline{L(n_1,...,n_P)}\right)_i - \left(\overline{L^{Path}}\right)_i}{\left(\overline{A_0 \exp\left(-\eta \sum_{p=1}^{P} k_p n_{p\min}\right)}\right)_i}, \tag{7a}$$

$$\tilde{\rho}_{i\max} = \frac{\left(\overline{L(n_1,...,n_P)}\right)_i - \left(\overline{L^{Path}}\right)_i}{\left(\overline{A_0 \exp\left(-\eta \sum_{p=1}^{P} k_p n_{p\max}\right)}\right)_i}, \tag{7b}$$

which represent the envelope of the possible values of the real reflectance (Fig. 4). The measurement channels are then defined to be those for which $\tilde{\rho}_{i\max} - \tilde{\rho}_{i\min} > \sigma_i$.

4.2.2 Saturated Channels

A channel is considered to be saturated if its radiance is below $3\sigma_{bi}$ (a factor of 3 is introduced in order to diminish the number of outliers). Within the 400-2500 nm spectral region, saturated channels are generally located near 1400 nm and 1900 nm, where H_2O strongly absorbs.

4.2.3 Reference Channels

The channels not selected as measurement or saturated channels are referred to as reference channels.

4.3 Surface Reflectance Estimator

This section describes the procedure used to estimate the surface reflectance from the radiance signal. In agreement with physical constraints and assumptions (see section 4.1), an estimator $\hat{\rho}_i$ of the surface reflectance in channel i is computed as

$$\hat{\rho}_i(\alpha) = \arg\min_{s\in\Omega}\left(\sum_{i=1}^{N} w_i(\tilde{\rho}_i - s(\lambda_i))^2 + \alpha\int_a^b s''(u)^2\,du\right) \tag{8}$$

where $\Omega=\{ s : s \in C^2[a,b],\ s'' \in L^2[a,b]\}$, s'' denotes the second derivative of s, w_i are weighting coefficients, $\alpha > 0$ is a regularization parameter, and $[a,b]$ contains all the λ_i values. The first term in equation (8) controls the fidelity to the data and the second term controls the global smoothness of the estimator. $\hat{\rho}_i$ is called a smoothing spline estimator and is known to be a natural cubic spline with knots at the observation points $\lambda_1,...,\lambda_N$ (Reinsch, 1967) (DeBoor, 1978) (Wahba, 1975) (Kimeldorf et al., 1970) (Wahba, 1978). A cubic smoothing spline with knots in $\lambda_1,...,\lambda_N$ is a piecewise cubic polynomial $s(\lambda)$ where pieces join C^2-continuously at the points $\lambda_1,...,\lambda_N$, i.e., $s(\lambda)$ and satisfies the conditions :

- On each interval $[\lambda_{i-1},\lambda_i]$, $i=1,...,N+1$, where $\lambda_0 = a$ and $\lambda_{N+1} = b$, $s(\lambda)$ is a polynomial of degree ≤ 3
- $s(\lambda)$ is C^2-continuous on $[a,b]$
- In addition, $s(\lambda)$ is called natural if it is linear on the end intervals $[a,\lambda_1]$ and $[\lambda_N,b]$

The weights w_i used to estimate the reflectance are given by:

- $w_i = 1/\sigma_i$ in the reference channels
- $w_i = 0$ in the measurement and saturated channels

The weights allow the noise on $\tilde{\rho}_i$ to be smoothed within the reference channels and to interpolate the reflectance elsewhere.

Equation (8) can be simplified if the natural cubic spline is represented with its value-second derivative form (Green et al., 1994). Let $\mathbf{S}$ denote the vector $[s(\lambda_1),...,s(\lambda_N)]^{\mathrm{T}}$ (the superscript T is matrix transposition) and $\mathbf{U}$ the vector $[s''(\lambda_2),...,s''(\lambda_{N-1})]^{\mathrm{T}}$ (by definition, a natural cubic spline has $s''(\lambda_1) = s''(\lambda_N) = 0$). Define $h_i = \lambda_{i+1} - \lambda_i$ for $i=1,...,N-1$, and let $\mathbf{Q}$ be a tridiagonal matrix $N\times(N-2)$ in size with entries $q_{i,i} = 1/h_i$, $q_{i+1,i} = -(1/h_i + 1/h_{i+1})$, $q_{i+2,i} = 1/h_{i+1}$, and $\mathbf{R}$ a tridiagonal matrix $(N-2)\times(N-2)$ in size with entries $r_{i,i} = (h_i + h_{i+1})/3$, $r_{i,i+1} = r_{i+1,i} = h_i/6$. $\mathbf{S}$ and $\mathbf{U}$ specify a natural cubic spline if and only if the condition $\mathbf{Q}^{\mathrm{T}}\mathbf{S} = \mathbf{R}\mathbf{U}$ is satisfied and then

$$\int_a^b s''(u)^2\,du = \mathbf{U}^{\mathrm{T}}\mathbf{R}\mathbf{U}. \tag{9}$$

By substituting $\mathbf{U}$ by $\mathbf{R}^{-1}\mathbf{Q}^{\mathrm{T}}\mathbf{S}$ in equation (9), equation (8) can be rewritten in matrix form as

$$\hat{\boldsymbol{\rho}}(\alpha) = \arg\min_{\mathbf{S}}((\tilde{\boldsymbol{\rho}} - \mathbf{S})^{\mathrm{T}} \mathbf{W}(\tilde{\boldsymbol{\rho}} - \mathbf{S}) + \alpha \mathbf{S}^{\mathrm{T}} \mathbf{Q} \mathbf{R}^{-1} \mathbf{Q}^{\mathrm{T}} \mathbf{S}) \tag{10}$$

where $\tilde{\boldsymbol{\rho}} = [\tilde{\rho}_1, ..., \tilde{\rho}_N]^{\mathrm{T}}$ and $\mathbf{W} = \mathrm{diag}[w_1, ..., w_N]$. Resolution of equation (10) yields

$$\hat{\boldsymbol{\rho}}(\alpha) = (\mathbf{W} + \alpha \mathbf{Q} \mathbf{R}^{-1} \mathbf{Q}^{\mathrm{T}})^{-1} \mathbf{W} \tilde{\boldsymbol{\rho}} . \tag{11}$$

By defining $\mathbf{A_0} = \mathrm{diag}[\left(\overline{A_0}\right)_1, ..., \left(\overline{A_0}\right)_N]$, we can infer from equation (6) that $\tilde{\boldsymbol{\rho}} = \mathbf{A}_0^{-1}(\mathbf{L} - \mathbf{L}^{\mathbf{Path}})$ where $\mathbf{L} = [\left(\overline{L(n_1, ..., n_P)}\right)_1, ..., \left(\overline{L(n_1, ..., n_P)}\right)_N]^{\mathrm{T}}$ and $\mathbf{L}^{\mathbf{Path}} = [\left(\overline{L^{Path}}\right)_1, ..., \left(\overline{L^{Path}}\right)_N]^{\mathrm{T}}$. Then, by defining $\mathbf{B} = (\mathbf{W} + \alpha \mathbf{Q} \mathbf{R}^{-1} \mathbf{Q}^{\mathrm{T}})^{-1} \mathbf{W} \mathbf{A}_0^{-1}$, the surface reflectance estimator $\hat{\boldsymbol{\rho}}$ can be expressed as a function of the measured radiance and the path radiance by

$$\hat{\boldsymbol{\rho}}(\alpha) = \mathbf{B}(\mathbf{L} - \mathbf{L}^{\mathbf{Path}}) . \tag{12}$$

We obtain a surface reflectance estimator for a given value of the smoothness parameter α.

α controls the tradeoff between the fidelity to the data and the global smoothness of the reflectance estimator. If it is too small, the model fits the noise and if it is too large then some of the original signal may be damped. In our study, the noise level σ_i is known and, therefore, the regularization parameter α can be determined using the discrepancy principle (Engl et al., 1996). A Newton's method is used to iteratively find the desired value of the parameter α.

4.4 Gas Concentrations Estimator

In this section, we compute simultaneously the estimates $\hat{n}_p$ of the P gases of interest as

$$(\hat{n}_p) = \arg\min_{n_p}(C(n_p)) , \tag{13}$$

$$\text{with } C(n_p) = \sum_{i=1}^{N} w_{bi} \left(\left(\overline{L(n_1, ..., n_P)}\right)_i - \hat{\rho}_i \left(\overline{A_0 \exp\left(-\eta \sum_{p=1}^{P} k_p n_p \right)} \right)_i - \left(\overline{L^{Path}}\right)_i \right)^2 ,$$

where $w_{bi} = 1/\sigma_{bi}$ in the measurement channels and $w_{bi} = 0$ elsewhere. We use a Newton's method for minimization to solve equation (13) for the $P \times 1$ estimated vector $\hat{\mathbf{n}} = [\hat{n}_1, ..., \hat{n}_P]^{\mathrm{T}}$. Indeed, this method is particularly adapted because equation (13) is strongly non-linear towards the n_p and because the $P \times 1$ Jacobian and the $P \times P$ Hessian matrices (resp., $\mathbf{J}$ and $\mathbf{H}$) can be computed analytically. The $P \times 1$ vector of increments $\boldsymbol{\Delta}\mathbf{n}$ is given by

$$\boldsymbol{\Delta}\mathbf{n} = -\mathbf{H}^{-1}\mathbf{J} \tag{14}$$

where $\mathbf{J}$ and $\mathbf{H}$ are equal to

$$\mathbf{J} = \begin{bmatrix} \frac{\partial C}{\partial n_1} \\ \frac{\partial C}{\partial n_2} \\ \vdots \\ \frac{\partial C}{\partial n_P} \end{bmatrix}, \qquad \mathbf{H} = \begin{bmatrix} \frac{\partial^2 C}{\partial n_1^2} & \frac{\partial^2 C}{\partial n_1 \partial n_2} & \cdots & \frac{\partial^2 C}{\partial n_1 \partial n_P} \\ \frac{\partial^2 C}{\partial n_2 \partial n_1} & \frac{\partial^2 C}{\partial n_2^2} & \cdots & \frac{\partial^2 C}{\partial n_2 \partial n_P} \\ \vdots & \vdots & \cdots & \vdots \\ \frac{\partial^2 C}{\partial n_P \partial n_1} & \frac{\partial^2 C}{\partial n_P \partial n_2} & \cdots & \frac{\partial^2 C}{\partial n_P^2} \end{bmatrix} . \tag{15}$$

Starting with $\hat{\mathbf{n}} = \mathbf{0}$, the process is iterated until convergence is reached, which is when the added increment $\boldsymbol{\Delta}\mathbf{n}$ leads to variations in the concentrations of the gases lower than a specified tolerance. Note that in practice, only the measurement channels are retained in the calculation.

5. VALIDATION OF SIMULATED DATA

This section describes the preliminary results obtained with the proposed method. JRGE has been compared with APDA for water vapor retrieval. For this comparison, the JPL and the Johns Hopkins University (JHU), Baltimore, MD, spectral libraries were employed. These databases consist of measured reflectance spectra for 430 mineral samples (from JPL), to which we added 41 soil samples, 45 manmade samples, 4 vegetation samples, and 5 water samples (from JHU). Radiance spectra were simulated using MODTRAN4 in the following conditions : aerosol-free US 1976 Standard Atmosphere Model with an excess of water vapor equal to 3500 ppm in the first atmospheric kilometer (to simulate a vapor plume), solar zenith angle of 40 degrees, a target at sea level and a nadir-viewing sensor located above the atmosphere. Radiances were then averaged according to the AVIRIS instrument specifications for the year 1995 and related system noise was added to the computed signals. Retrieval of the water vapor content was performed both with the 3-channel optimal APDA technique (reference channels : 875.25 nm / FWHM = 8.86 nm and 1000.13 nm / FWHM = 9.01 nm, measurement channel : 942.49 nm / FWHM = 8.95 nm) and the proposed JRGE method. For comparison with APDA, which estimates the total gas column, we define the retrieval error $E(p)$ in the gaseous species p relatively to the total amount by

$$E(p) = \frac{n_p - \hat{n}_p}{N_{0p} + n_p}. \tag{16}$$

Results are reported in Table 1.

Table 1. Comparison between APDA and JRGE for water vapor retrieval. JRGE significantly reduces error in H_2O estimate for a set of widespread surface materials yielding APDA particularly large errors (Borel et al., 1996) (Schläpfer et al., 1998). JRGE enhancement factor is 2.5 for whole database (see text for details).

Material	APDA Error (%)	JRGE Error (%)
CUMMINGTONITE-IN-6A	-6.18	-0.12
ENSTATITE-IN-10B	-40.79	5.94
FAYALITE-NS-1A	-5.45	0.61
HEMATITE-FE2602	11.47	-2.92
MOLYBDENITE-S-11A	19.71	1.06
SIDERITE-COS2002	-31.81	4.45
TRIPHYLITE-P-4A	-42.13	-3.60
Database	APDA RMSE (%) : 7.10	JRGE RMSE (%) : 2.87

For the seven materials yielding the largest errors for APDA, the spectral shape of the reflectance within the 940 nm water vapor absorption band is fitted by the JRGE method (Fig. 2) with an accuracy of a few percent; the quality of the resulting determination of water vapor content is enhanced by a 8.4 average factor. For the whole database, the accuracy of JRGE for water vapor retrieval is 2.87%, yielding a 2.5 enhancement factor.

6. CONCLUSION

We have developed a comprehensive method to retrieve both ground reflectances and trace gas amounts from hyperspectral remotely sensed data. The method yields an enhancement factor equal to 2.5 in H_20 retrieval accuracy in comparison with conventional methods. The method can thus be also used to enhance existing atmospheric correction techniques for ground based applications (e.g., geology). Improved accuracy should allow the monitoring of numerous geophysical phenomena with relatively low gas emission.

7. REFERENCES

Borel, C. C. and D. Schläpfer (1996). Atmospheric Pre-Corrected Differential Absorption Techniques To Retrieve Columnar Water Vapor : Theory and Simulations. 6th Annual JPL Airborne Earth Science Workshop, Jet Propulsion Laboratory, Pasadena, CA.

Bruegge, C. J., J. E. Conel, J. S. Margolis, R. O. Green, G. Toon, V. Carrère, R. G. Holm and G. Hoover (1990). In-situ atmospheric water-vapor retrieval in support of AVIRIS validation. Imaging Spectroscopy of the Terrestrial Environment. Orlando, FL. **1298:** 150-163.

Carrère, V. and J. E. Conel (1993). "Recovery of Atmospheric Water Vapor Total Column Abundance from Imaging Spectrometer Data Around 940 nm - Sensitivity Analysis and Application to Airborne Visible/Infrared Imaging Spectrometer (AVIRIS) Data." Remote Sens. Environ. **44**: 179-204.

Curran, P. J. (1994). Imaging Spectrometry - Its Present and Future Rôle in Environmental Research. Imaging Spectrometry - a Tool for Environmental Observations. J. Hill and J. Mégier, ECSC, EEC, EAEC, Brussels and Luxembourg. Printed in The Netherlands**:** 1-23.

De Jong, S. M. and T. G. Chrien (1996). Mapping Volcanic Gas Emissions in the Mammoth Mountain Area using AVIRIS. 6th Annual JPL Airborne Earth Science Workshop, Jet Propulsion Laboratory, Pasadena, CA.

DeBoor, C. (1978). A practical guide to splines. New York.

Engl, H. W., M. Hanke and A. Neubaur (1996). Regularization of Inverse Problems, Kluwer Academic Publishers.

Esaias, W. (1986). Moderate resolution imaging spectrometer. Earth Observing System. NASA, Washington D.C. **IIb:** 49-53.

Frouin, R., P.-Y. Deschamps and P. Lecomte (1990a). "Determination from Space of Atmospheric Total Water Vapor Amounts by Differential Absorption near 940 nm : Theory and Airborne Verification." J. Appl. Meteorol. **29**: 448-460.

Frouin, R. and E. Middleton (1990b). A Differential Absorption Technique to Estimate Atmospheric Total Water Vapor Amounts. American Meteorological Society Symposium on the First ISLSCP Field Experiment (FIFE), Anaheim, CA.

Gao, B.-C. and A. F. H. Goetz (1990). Determination of total column water vapor in the atmosphere at high spatial resolution from AVIRIS data using spectral curve fitting and band ratioing techniques. Imaging Spectroscopy of the Terrestrial Environment. Orlando, FL. **1298:** 138-149.

Goetz, A. F. H. (1992). Imaging Spectrometry for Earth Remote Sensing. Imaging Spectroscopy : Fundamentals and Prospective Applications. F. Toselli and J. Bodechtel, ECSC, EEC, EAEC, Brussels and Luxembourg. Printed in The Netherlands**:** 1-19.

Green, P. J. and B. W. Silverman (1994). Nonparametric Regression and Generalized Linear Models. London.

Green, R. O., V. Carrère and J. E. Conel (1989). Measurement of Atmospheric Water Vapor using the Airborne Visible/Infrared Imaging Spectrometer. Image Processing '89, Sparks, NV, American Society for Photogrammetry and Remote Sensing.

Green, R. O., J. E. Conel, J. S. Margolis, C. Chovit and J. Faust (1996a). In-Flight Calibration and Validation of the Airborne Visible/Infrared Imaging Spectrometer (AVIRIS). 6th Annual JPL Airborne Earth Science Workshop, Jet Propulsion Laboratory, Pasadena, CA.

Green, R. O., D. A. Roberts and J. E. Conel (1996b). Characterization and Compensation of the Atmosphere for the Inversion of AVIRIS Calibrated Radiance to Apparent Surface Reflectance. 6th Annual JPL Airborne Earth Science Workshop, Jet Propulsion Laboratory, Pasadena, CA.

Kaufman, Y. J. and B.-C. Gao (1992). "Remote Sensing of Water Vapor in the Near IR from EOS/MODIS." IEEE Trans. Geosci. Remote Sensing **30**(5): 871-884.

Kimeldorf, G. and G. Wahba (1970). "A correspondence between Bayesian estimation on stochastic processes and smoothing by splines." Ann. Inst. Statist. Math. **41**: 495-502.

Liou, K.-N. (1980). An Introduction to Atmospheric Radiation, Academic Press, Inc.

Reinsch, C. H. (1967). "Smoothing by Spline Functions." Numer. Math. **10**: 177-183.

Rothman, L. S., C. P. Rinsland, A. Goldman, S. T. Massie, D. P. Edwards, J.-M. Flaud, A. Perrin, C. Camy-Peyret, V. Dana, J.-Y. Mandin, J. Schroeder, A. Mccan, R. R. Gamache, R. B. Wattson, K. Yoshino, K. V. Chance, K. W. Jucks, L. R. Brown, V. Nemtchinov and P. Varanasi (1998). "THE HITRAN MOLECULAR SPECTROSCOPIC DATABASE AND HAWKS (HITRAN ATMOSPHERIC WORKSTATION) : 1996 EDITION." J. Quant. Spectrosc. Radiat. Transfer **60**(5): 665-710.

Schläpfer, D., C. C. Borel, J. Keller and K. I. Itten (1996a). Atmospheric Pre-Corrected Differential Absorption Techniques to Retrieve Columnar Water Vapor : Application to AVIRIS 91/95 Data. 6th Annual JPL Airborne Earth Science Workshop, Jet Propulsion Laboratory, Pasadena, CA.

Schläpfer, D., C. C. Borel, J. Keller and K. I. Itten (1998). "Atmospheric Precorrected Differential Absorption Technique to Retrieve Columnar Water Vapor." Remote Sens. Environ. **65**: 353-366.

Schläpfer, D., J. Keller and K. I. Itten (1996b). Imaging Spectrometry of Tropospheric Ozone and Water Vapor, A. A. Balkema, Rotterdam.

Vane, G., W. M. Porter, H. T. Enmark, S. A. Macenka, M. P. Chrisp, T. G. Chrien, L. Steimle, G. C. Bailey, D. C. Miller, J. S. Bunn, R. E. Steinkraus, R. W. Hickok, J. H. Reimer, J. R. Heyada, S. C. Carpenter, W. T. S. Deich, M. Lee and E. A. Miller (1987). Airborne Visible/Infrared Imaging Spectrometer (AVIRIS) - A Description of the Sensor, Ground Data Processing Facility, Laboratory Calibration, and First Results.

Wahba, G. (1975). "Smoothing noisy data with spline functions." Numer. Math. **24**: 383-393.

Wahba, G. (1978). "Improper priors, spline smoothing, and the problem of guarding against model errors in regression." J. Roy. Statist. Soc. **40**(B).